university of groningen / Faculty of Science and Engineering / Applied Physics & Physics

Transport of mendelevium ions through the NEXT ion guide

Maarten Mijland
s3099474

July 2021

Bachelor thesis physics
Student: M.K. Mijland
First supervisor: dr. J. Even
Second assessor: dr. T. Schlathölter

Abstract

The NEXT project aims to study Neutron-rich EXotic nuclei produced in nuclear Transfer reactions. The studies of such exotic nuclei require an efficient ion transport and sample preparation. Within the framework of this thesis, ion optical simulation studies of a novel ring-based ion guide were performed in order to find electrical settings suitable for $^{261}Md^{1+}$ and $^{261}Md^{2+}$. In these studies, electrical optimum settings were found that allow a transmission yield of 90% for mendelevium ions. The mechanical tolerance of the apparatus was also investigated in simulation studies, which can be used as a guideline for manufacturing the ion guide and placing it inside the NEXT setup.

Contents

1 Introduction

1.1 Neutron-rich heavy nuclei

Nuclear stability has limitations which can arise from an excess of protons, neutrons or even a high mass. According to the liquid drop model, nuclei are limited to a proton number of Z≈100 which is the element fermium [1]. That means that other theories describing nuclear stability are necessary to explain the existence of nuclei heavier than fermium. These nuclei can be created using multi-nucleon transfer reactions, which have the highest cross-sections to access nuclei in the neutron-rich heavy element region [2]. A heavy ion beam is impinged at energies around the Coulomb barrier on an actinide target. During the deep-inelastic collisions of the projectile and the target nucleons are exchanged resulting in two transfer fragments (see Figure 1). This technique has already been used to successfully produce several neutron-rich species of nuclei in the past with Z ≤103 (e.g. ^{260}Md, ^{261,262}Lr) that are not accessible to the conventional fusion reactions [3]. On the nuclear chart (figure 2) many nuclides in the top right corner are coloured in red, meaning their masses are only known through theoretical extrapolation, especially on the right(neutron-rich) side. The black circle on the graph indicates an accessible region by MNTs. In my thesis, I focused on the ion optical simulation of the sample preparation of ^{261}Md, which is so far undiscovered but is predicted to be accessible in the transfer reaction ^{48}Ca+^{248}Cm→ ^{261}Md+X.

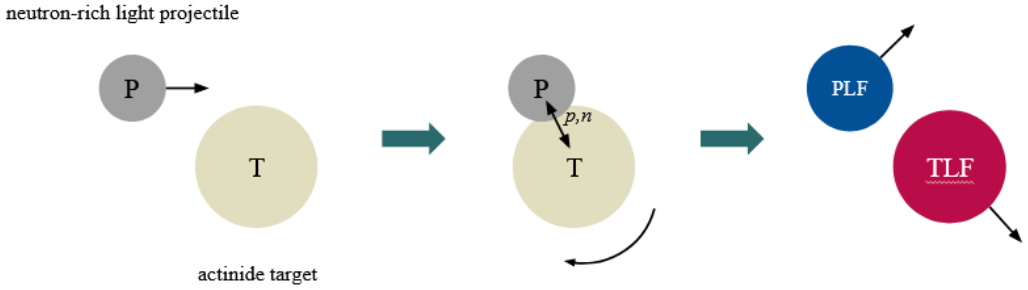

Figure 1: The process of a multi-nucleon transfer reaction, a projectile (P) will graze a target (T) and transfer some of its nucleons to create a light projectile-like fragment(PLF) and a heavy target-like fragment(TLF)[4]

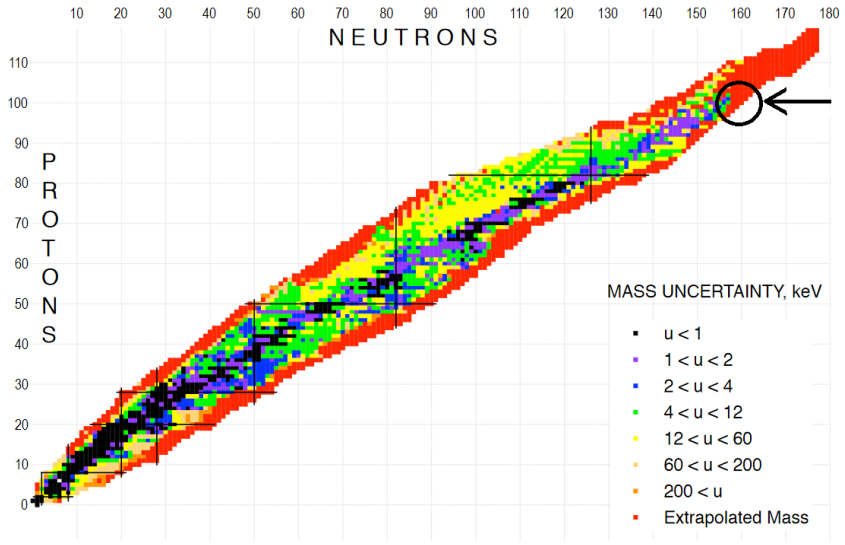

Figure 2: The nuclear chart featuring mass uncertainty according to the latest Atomic Mass Evaluation, AME2020. The masses of nuclei highlighted in red are only known through extrapolations. [5]

1.2 NEXT

The NEXT project has the goal of measuring the masses and decay properties of Neutron-rich, EXotic, heavy nuclei produced in multi-nucleon Transfer reactions. The primary beam is delivered by the AGOR cyclotron at the University of Groningen. The beam is focused onto a target to initiate MNTs. The multi-nucleon transfer reaction products have a large angular distribution, which makes experimentally studies of transfer products challenging. To solve this problem, the target material will be placed inside a large solenoid magnet, which will be able to separate the target-like fragments from the projectile-like fragments[6]. A beam dump will be placed behind the target which will catch the non-reacted beam as illustrated in Figure 3.

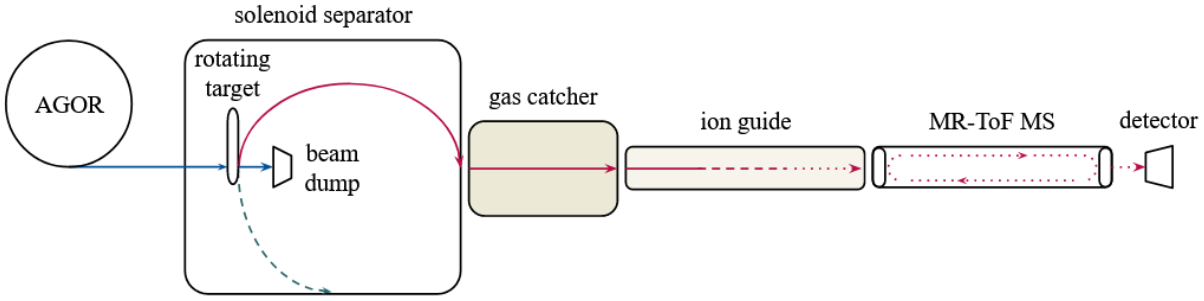

Figure 3: Schematic of the NEXT setup, the red arrows indicate the trajectory of the target-like fragments. The blue arrows indicate the projectiles and the green dashed arrow indicate the projectile-like fragments.[4]

The target-like fragments will be steered by the magnetic field into the gas catcher. In the helium filled gas catcher, they will be slowed down through collisions with the gas [7]. The ions are guided by DC field towards the RF carpet, and then by DC and RF field towards the central hole in the RF carpet.

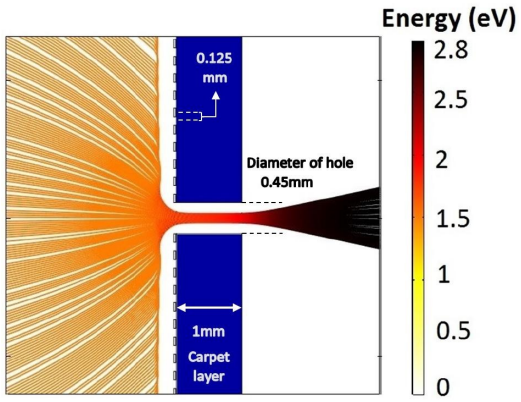

Figure 4: The trajectories of ions through the hole in the RF-carpet at the end of the gas catcher.[7]

The ions are ejected from the gas-catcher through a supersonic gas jet, as indicated in Figure 4. The ions will be transported by the ion guide from the gas catcher to the Multi-Reflection Time-of-Flight Mass Spectrometer (MR-ToF MS). The ions that leave the gas catcher have relatively low energies (eV), the beam profile is divergent and continuous. In the ion guide the ions will be focused, bunched and accelerated to relatively high energy(keV) for injection into the MR-ToF MS. The pressure in the gas catcher is 50 mbar and in the MR-ToF MS the pressure is 10^{-9} mbar. In order to couple these 2 pressure regions, there will be 2 intermediate steps. The pressure in the ion guide will be 10^{-3} mbar, followed by a lens section with 10^{-6} mbar.

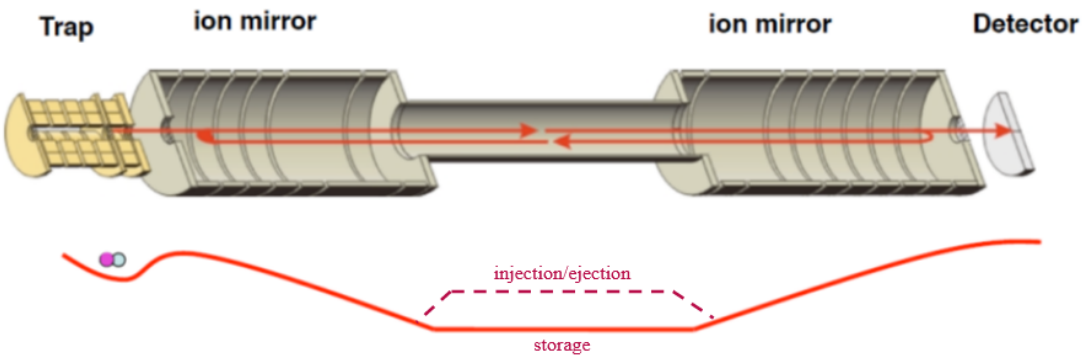

Figure 5: Schematic of the MR-ToF MS with the trajectories of the ions. The red line indicates the shape of the electric potential inside the MR-ToF MS[4]

The MR-ToF MS is basically a tube with on either end an electrostatic ion mirror which reflects the ions back and forth many times so that they travel a longer path. As the ions travel, they will separate based on their different mass-to-charge ratios. At some point, the ions are ejected by a potential lift in the center of the MR-ToF MS and registered by a detector. The mass differences can be determined based on the time-of-flight differences. The more laps the ions have travelled, the higher resolving power the MR-ToF MS has(10^{5-6})[8].
The ion guide that will couple the gas catcher and the MR-ToF is under development A detailed description of the conceptual design of the ion guide is presented in chapter 3. Within this thesis, ion optical simulations were performed in order to find optimum parameters for the ion guide, as well as simulations to determine the tolerance with which the ion guide should be built within the setup.

2 Theory

the ion guide will trap ions using electric fields alternating at radio frequency. In this chapter, the theory behind that technique is discussed in more detail.

2.1 Trapping ions using RF fields

The equation of motion for a charged particle in electric and magnetic fields is given by

$$m\ddot{\mathbf{r}} = q\mathbf{E}(\mathbf{r},t) + q\dot{\mathbf{r}} \times \mathbf{B}(\mathbf{r},t) \tag{1}$$

Where q is the charge of the ion, m the mass of the ion and $\mathbf{E}$ and $\mathbf{B}$ the electric and magnetic fields. For the purposes of the ion guide, we can assume that there are weak electric fields and heavy particles with low kinetic energies. This means that the velocity $\dot{\mathbf{r}}$ is very small in comparison to the velocity of light, and as a result, the weak force exerted by the magnetic field can be disregarded. A radio frequency electric field can be used to apply a force to charged particles known as the ponderomotive force [9]. This effect is able to push ions towards a region of weaker field. In a homogeneous oscillating electric field, ions will oscillate harmonically with the electric field(see Figure 6 C). When the field is inhomogeneous, the ion experience more force the closer they are to the strong field. After ions are pushed away from the strong field, they enter a region of weaker electric field, where they are then pulled towards the electrode again with less force. As a result, they do not move as close to the electrode as they originally did. This is illustrated in Figure 6 D.

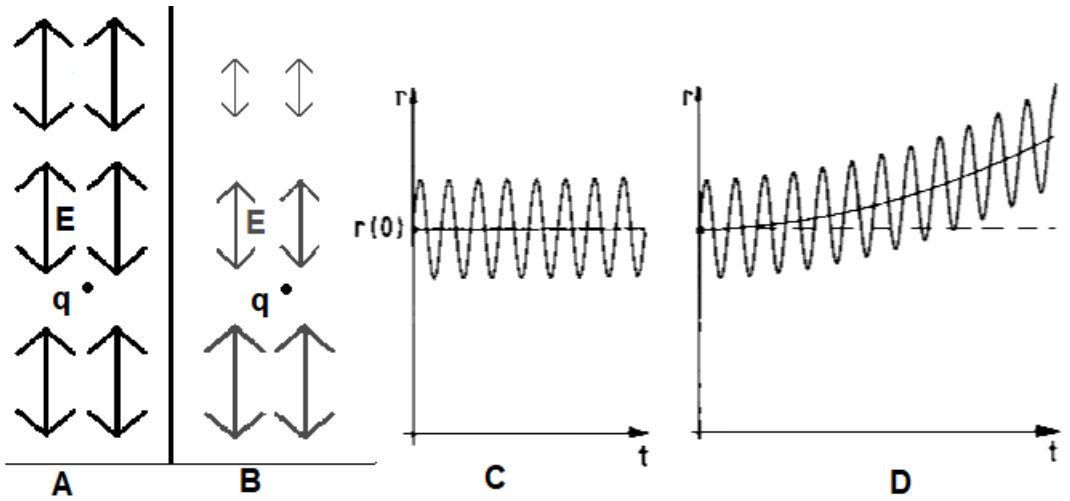

Figure 6: A) An ion q in a homogeneous oscillating electric field. B) An ion q in an inhomogeneous oscillating electric field. C) The motion of an ion in a homogeneous oscillating electric field. D) The motion of an ion in an inhomogeneous oscillating electric field. [9]

If the field varies smoothly as a function of the coordinate r, and the frequency is high enough to keep the amplitude of the oscillations **a** small, which is defined in equation 2, then the motion of the ions can be described by 2 parts the rapidly oscillating part $\mathbf{R}_1$ and the non-oscillating part $\mathbf{R}_0$ (see equation 3).

$$\mathbf{a} = \frac{q\mathbf{E_0}}{m\Omega^2} \tag{2}$$

where $\mathbf{E_0}$ is the amplitude of the oscillating field and Ω the angular frequency of the oscillating field.

$$\mathbf{r}(t) = \mathbf{R_0}(t) + \mathbf{R_1}(t) \tag{3}$$

The motion of interest is mainly $\mathbf{R}_0$, which is described by the equation

$$m\ddot{\mathbf{R}}_\mathbf{0} = -\frac{q^2}{4m\Omega^2}\nabla\mathbf{E}_0^2 \tag{4}$$

This equation shows that the ions are always attracted to the region of weaker field because it experiences a force caused by the inhomogeneity of the field, the direction and strength of which is determined by the gradient of $\mathbf{E}_0^2$. The force is also proportional to the squared charge, which means that the sign of the charge does not matter. If one accounts for an electrostatic field on top of the oscillating field, a potential can be derived.

$$V^*(\mathbf{R}_0) = \frac{q^2(E_0(R_0))^2}{4m\Omega^2} + q\Phi_s(R_0) \tag{5}$$

with V^* being called the effective potential or pseudopotential and Φ_s being an electrostatic potential. The equation of motion for $\mathbf{R}_0$ can now be written in terms of the pseudopotential.

$$m\ddot{\mathbf{R}}_\mathbf{0} = -\nabla V^*(\mathbf{R}_0) \tag{6}$$

The total energy of the ion can be found by integrating equation (6)

$$\frac{1}{2}m\dot{\mathbf{R}}_\mathbf{0}^2 + \frac{q^2(E_0(R_0))^2}{4m\Omega^2} + q\Phi_s(R_0) = E_m \tag{7}$$

This shows that the total energy of the ion is a constant, indicating that there is no energy being transferred to the ion from the oscillating field. This means that the average total energy is an adiabatic constant of motion. This only works based on the assumption that the fast oscillatory motion can be separated from

the slower non-oscillatory motion of the ion. It is possible to quantify the accuracy of this assumption using the adiabaticity parameter η defined by:

$$\eta = 2q\frac{|\nabla E_0|}{m\Omega^2} \tag{8}$$

A good way to test if the adiabatic approach holds for a given geometry is to see if along a typical ion trajectory η will not be above the maximum allowed value.

$$\eta_m = max[\eta_{mi}] = 0.3 \tag{9}$$

2.2 Trapping ions in a ring electrode RF-field

A ring electrode trap is a stack of ring-shaped electrodes with RF oscillating potential. Adjacent rings have opposite potential(see Figure 7). For a ring electrode trap the pseudopotential without any static potentials is given by:

$$\Phi_0 = \frac{q^2V_0^2k^2}{4m\Omega^2I_0^2(kr_0)}[I_1^2(kr)\cos(kz) + I_0^2(kr)\sin(kz)] \tag{10}$$

Where Φ_0 is the pseudopotential, 2πk is the distance between two rings of equal potential, r_0 the inner radius of the rings, z the axial distance, r the radial distance and I_0 and I_1 are modified Bessel functions of the first kind with orders 0,1 respectively. The pseudopotential strongly increases close to the electrodes. This can be seen in Figure 8

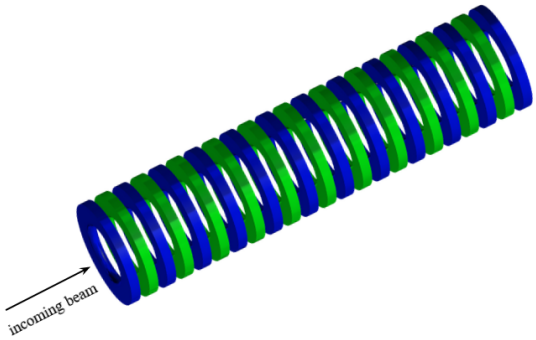

Figure 7: Ring electrode ion trap

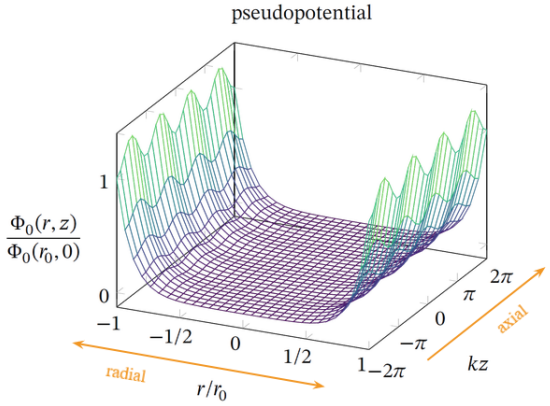

Figure 8: A visualization of the pseudopotential, which rapidly increases towards the inner diameter of the ring electrodes.

2.3 Transporting ions

Inside the ion guide will be a buffer gas that will slow down the ions. After the ions have been slowed down, they have to be transported towards the end of the ion guide where they can be ejected. To transport the ions, a travelling wave will be added on top of the confining RF potential. Every 4th ring will have the same lifted potential pertains for a while and advances by one ring continually (see Figure 9). This will move the ions forwards. Near the end of the ion guide, the travelling wave ends and the ions will be collected in a common place, waiting to be ejected.

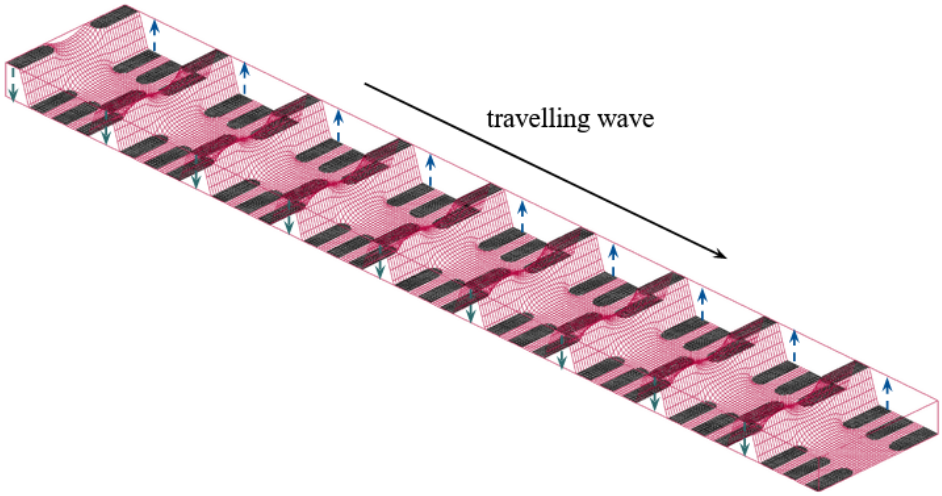

Figure 9: Schematic of the travelling wave that will transport the ions.

3 Design of the ion guide

The main purpose of the ion guide is to focus the continuous ions coming from the gas catcher and to and bunch them together in order to inject them into the MR-ToF MS. The ion guide is 193 mm long and consists of a stack of 78 ring electrodes of varying thickness and inner diameter. The spacings between the ring electrodes are slightly different depending on the axial position, but all around 1 mm. The ion guide is placed inside a vacuum chamber filled with helium gas at a pressure in the order of magnitude of 10^{-3}mbar. At this pressure, the gas will slow down the ions in the ion guide to thermal energy and provide an intermediate pressure region between the gas catcher and the MR-ToF MS. Every ring will be driven by a square-wave RF at a frequency of 3.82 MHz. The amplitude of this potential is the confining voltage. Adjacent rings will have opposite potentials. At each end of the ion guide is a 0.5 mm thick ring that is grounded to shield the outside from the RF-field, which were excluded in the 78 rings mentioned before.

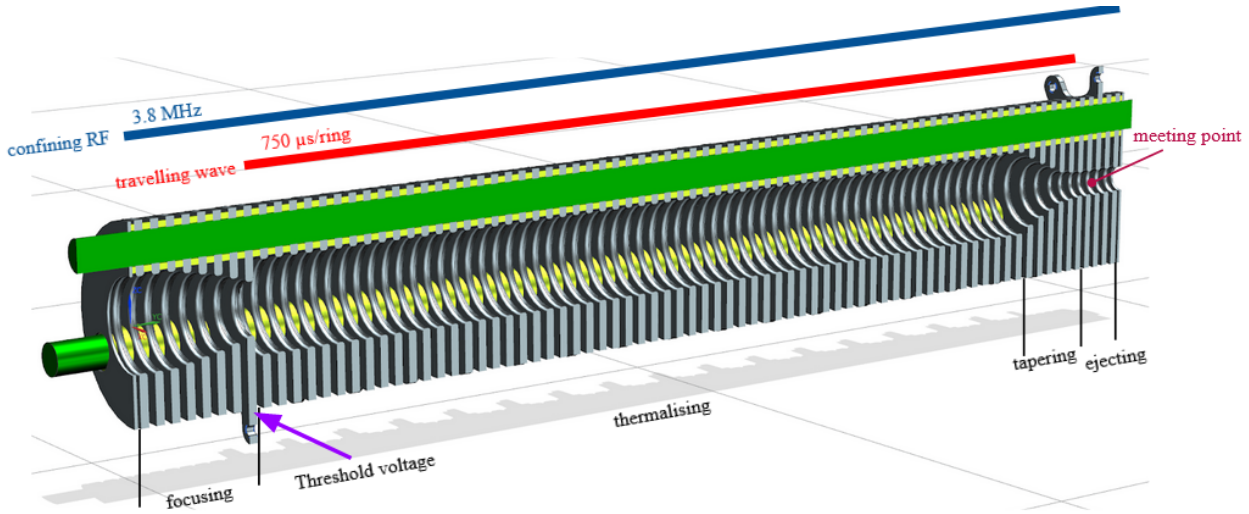

Figure 10: A cutaway view of the ion guide. Ions will travel from left to right.

3.1 The sections of the ion guide

3.1.1 Focusing

Ions will come in from the left side of Figure 10. The first section of the ion guide is the focusing section, which consists of 8 rings that slowly decrease in inner diameter from 14 mm to 8 mm. The final ring of the focusing section, which will be at an increased potential in order to create a barrier which only ions with high enough kinetic energies can pass through, such as the ions coming from the gas jet but not the thermalised ions from inside the ion guide. This increased potential is referred to as the threshold voltage, because only ions that meet a certain threshold of kinetic energy can pass it.

3.1.2 Thermalising

Behind the focusing section is the thermalising section of the ion guide. This section consists of 60 rings that are 1.3 mm thick and have an inner diameter of 14 mm. Here, the ions will lose kinetic energy by colliding with the helium gas present in the ion guide. The travelling wave in this section will transport the ions forward.

3.1.3 Tapering

Behind the thermalising section is the tapering section which consists of 6 rings which taper from an inner diameter of 14 mm to 4 mm. The thickness of the rings decreases here from 1.3 mm to 1.1 mm.

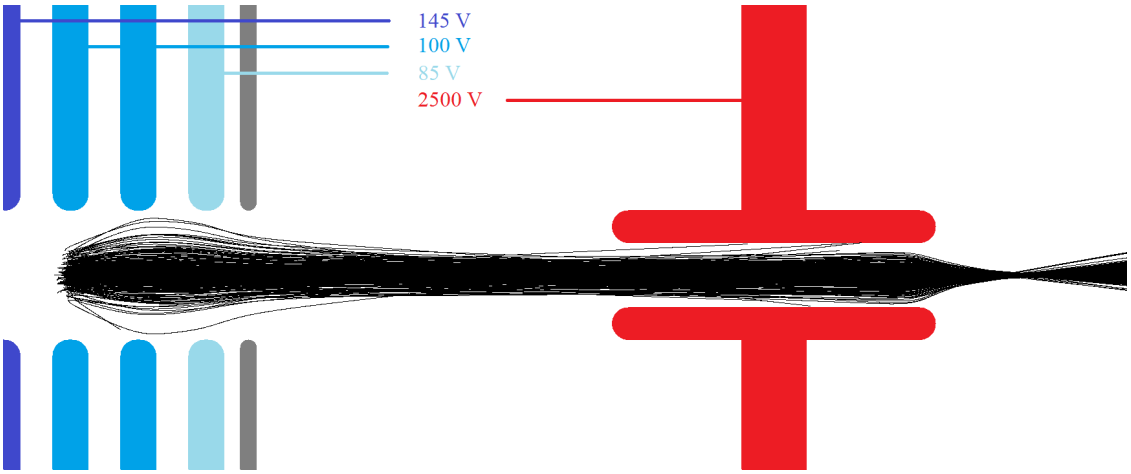

Figure 11: Ejection of ions from the ion guide, with indication of the voltages the final rings of the ion guide will get

3.1.4 Ejecting

Behind the tapering section, there is no travelling wave, so the ions will stop travelling forwards. Therefore, ions can start to accumulate at the meeting point, which is at the 3rd ring from the right(see Figure 11). Finally, after collecting a bunch of ions at the meeting point they are ejected by turning off the RF field at the final 4 electrodes and pulsing them to 145 V, 100 V, 100 V and 85 V respectively. This creates an electric field gradient accelerating the ions towards the drift tube which is located behind the ion guide and has an inner diameter of 2 mm. One purpose of the drift tube to separate the pressure region of the ion guide which is around 10^{-3} mbar from the lower pressure region of around 10^{-6} mbar behind the tube. The other purpose of the drift tube is to focus and accelerate the ions. This is done by applying a pulse of 2500 V to the drift tube as the ions reach the center of the drift tube. This creates high energetic, focused ion bunches that can be injected into the MR-ToF MS.

4 Simulations

4.1 SIMION

The software that was used to simulate the ions was SIMION. The geometry of the ion guide as well as the program that generates the potentials within SIMION was provided Xiangcheng Chen. This section gives an overview of the simulation studies.

4.2 Ion sample

The goal of this research was to investigate whether the ion guide which was originally optimised for iridium ions could also be used for the transport of heavier mendelevium ions. The mendelevium ions that exit the gas catcher through the RF carpet are expected to have charge state 1+ or 2+. The isotope of interest was mendelevium-261, which has a mass of 261.105 u [10]. The ions that leave the hole in the RF carpet are expected to have an angular distribution, which is illustrated in Figure 4. The ions in the sample have a kinetic energy of 2.59 eV to 2.68 eV.

4.3 Optimizing the ion guide for mendelevium

The ion guide has several electrical settings that can be varied. These are the RF frequency, the confining RF voltage, the travelling wave voltage and the threshold voltage. The transmission rate of the ion guide depends on the electrical settings and the type of ions. This section is about optimising the electrical settings of the ion guide for $^{261}Md^{1+}$ and $^{261}Md^{2+}$.

Table 1: Yield of the ion guide with proportionally scaled settings

Ion	Confining voltage	Travelling wave voltage	Threshold voltage	Yield
$^{261}Md^{1+}$	105.47 V	3.216 V	1.672 V	68.3 %
$^{261}Md^{2+}$	52.735 V	1.608 V	0.836 V	66 %

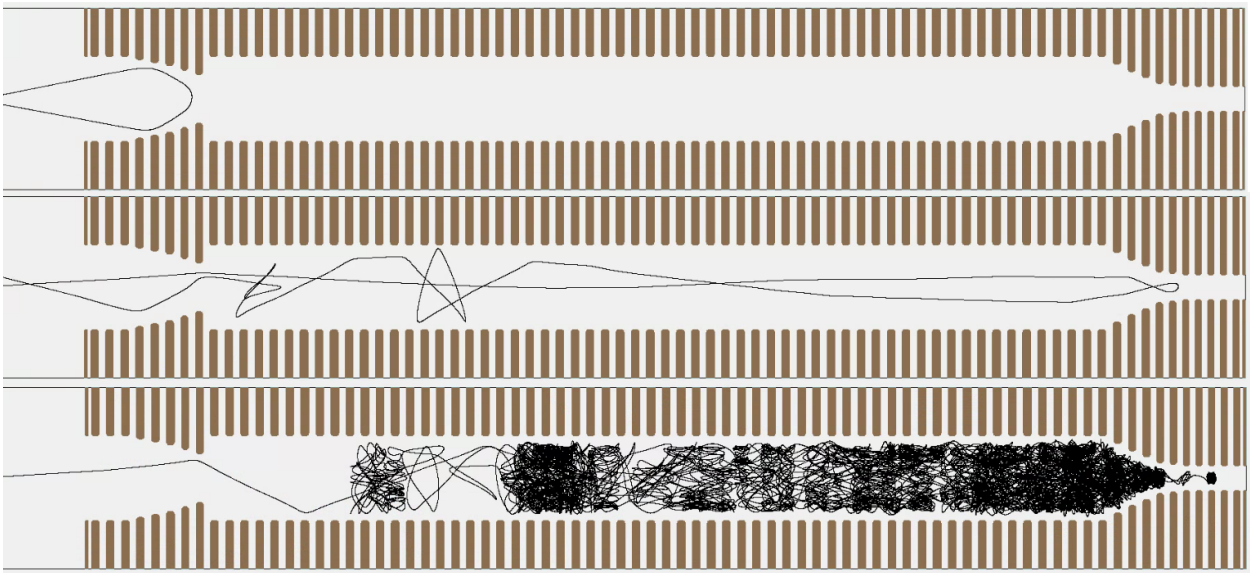

Figure 12: 3 example ion trajectories, The top is rejected in the focusing section, The middle bounces out of the ion guide, The bottom makes it all the way to the meeting point

4.3.1 Scaling the voltages

The ion guide was originally optimized for $^{203}Ir^{1+}$. As a first step to adjust the ion guide to $^{261}Md^{1+,2+}$, the voltages were increased proportionally to the mass-to-charge ratio. The RF-frequency was kept constant at 3.82MHz. The ions were injected from 15 mm distance into the ion guide.

These results are based on one sample of 300 ions. The simulations took over a day, which is why a single simulation was done for each charge state.

4.3.2 Injecting ions into the ion guide

The most common way ions were rejected was by bouncing out of the ion guide from the thermalising section. This can be prevented by increasing the threshold voltage. The problem with increasing the threshold voltage however is that if it is too high, ions will not be able to pass into the thermalising section of the ion guide.

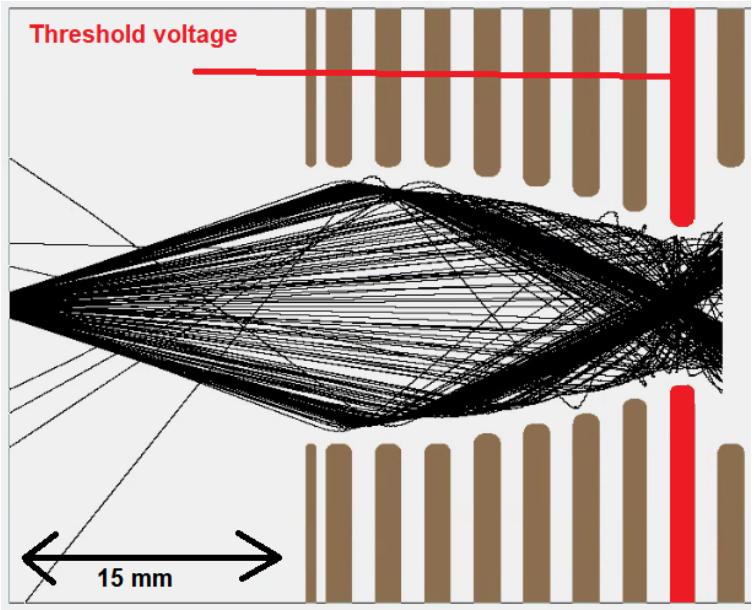

Figure 13: Trajectories of ions going being injected into the ion guide.

The impact of the threshold voltage on the ion injection yield was investigated systematically by simulations. The results are summarised in Figure 14. For this simulation, ions only had to reach the thermalisation section of the ion guide, therefore the process took 2 to 3 minutes. It is then possible to repeat the simulation for three times per threshold voltage and charge state. From these three simulations, a statistical error was determined.

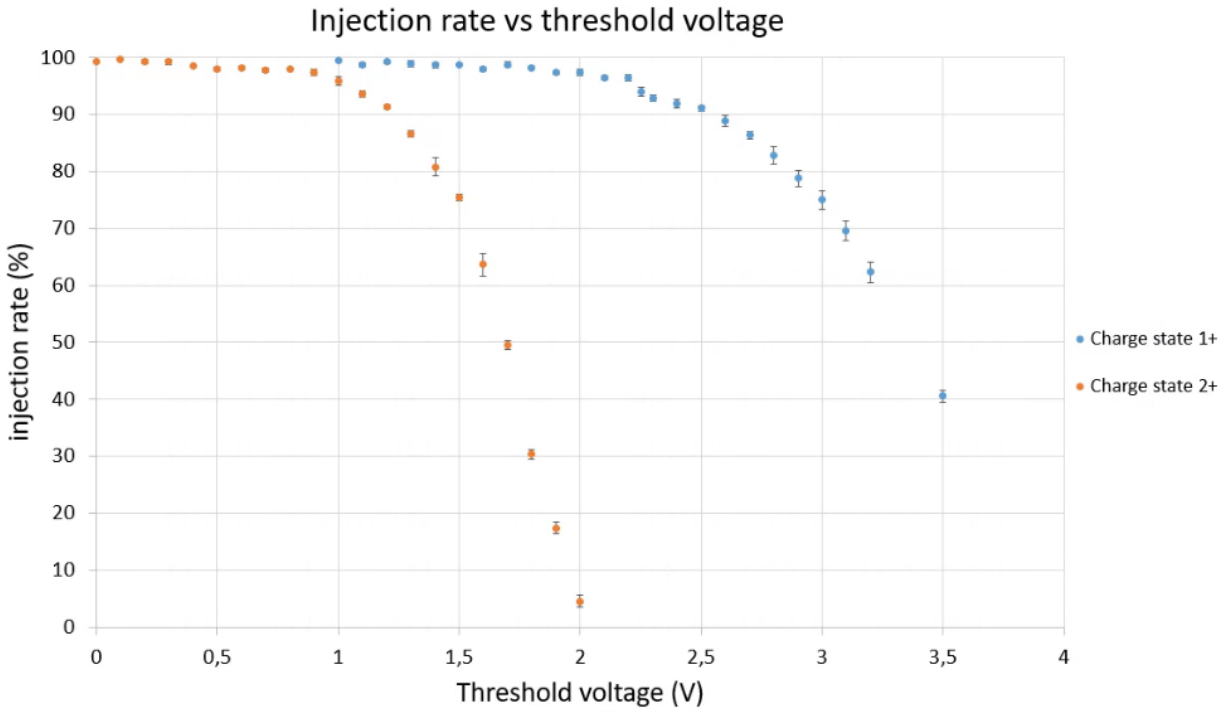

Figure 14: Dependence of the injection yield on the threshold voltage.

Table 2: The yield of ions for settings with increased threshold voltage

Ion	Confining voltage	Travelling wave voltage	Threshold voltage	Yield
$^{261}Md^{1+}$	105.47 V	3.216 V	2.2V	84.7 %
		2.5 V	2.0V	91.7 %
$^{261}Md^{2+}$	52.735 V	1.25 V	1 V	89.7 %

A simulation was done at a higher threshold voltage to see if a higher yield was achieved. Even with an increased threshold voltage, some ions would still be rejected after passing the potential barrier. A possible reason might be the travelling wave voltage was too high and that caused the bouncing back of the ions. Therefore, a simulation with lower travelling wave voltage was also done.

4.4 Impact of the kinetic energies of the ions on the acceptance of the ion guide

The ion sample that has been used for the tests so far consists of ions that leave the gas catcher with a kinetic energy of 2.59 eV to 2.68 eV. In the case that the ions leave the gas catcher with a different kinetic energy, it is interesting to study if the ion guide still functions. Therefore, simulations were done for ions that have different kinetic energies. For these simulations, the same angular distribution was used, but the kinetic energy of the ions was set to a fixed value and the voltage settings with the highest yield from Table 2 were used. Figure 15 shows that the ion-guide can accept ions with energies from 2.4 eV to 3.0 eV at a rate higher than 90%. If the kinetic energy of the ions is too low, they won't be able to pass the potential barrier and will thus be reflected. Ions with a kinetic energy that is too high can hit an electrode or bounce back and pass the potential barrier.

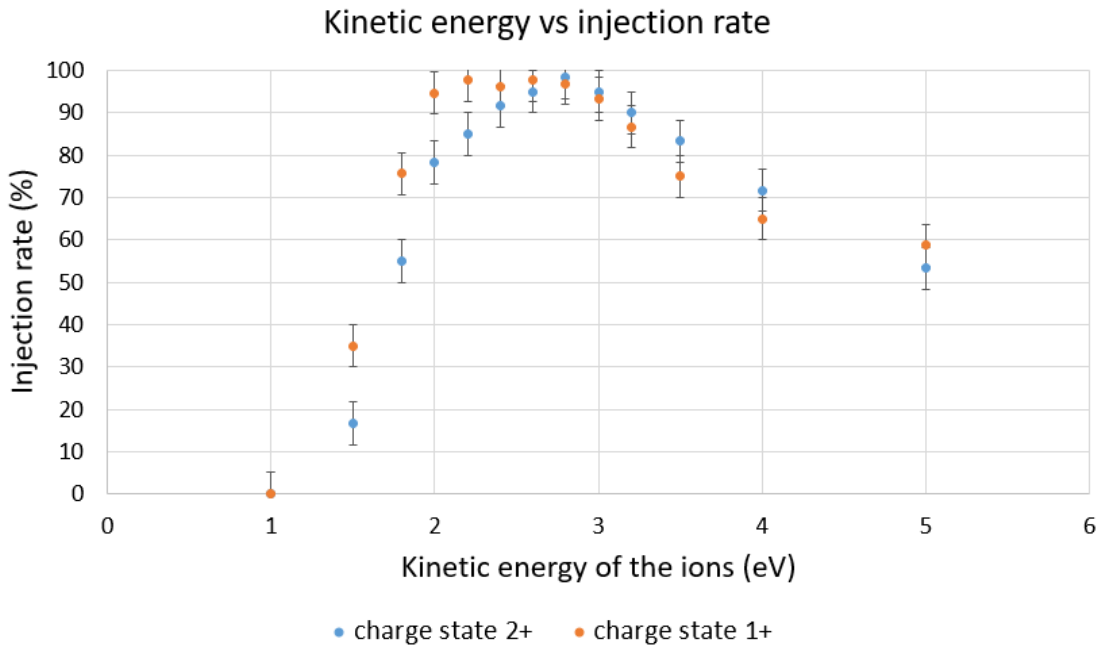

Figure 15: Dependence of the yield of the ion guide on the kinetic energy of the ions.

These simulations took around 40-45 minutes each because ions need time to thermalise. That is why only one sample of ions was used for each point in Figure 15 and the error bars are an estimation.

To prevent ions from hitting electrodes, the confining voltage can be adjusted. A test was done to find the minimum required confining voltage for which ions at a certain kinetic energy will not hit electrodes. This was done by increasing the confining voltage in steps of 5 until the point the ions would stop hitting electrodes.

Table 3: Minimum confining voltages depending on kinetic energies of the ions

Kinetic Energy	Minimum confining voltage $^{261}Md^{1+}$	Minimum confining voltage $^{261}Md^{2+}$
1 eV	50 V	30 V
2.6 eV	90 V	45 V
5 eV	120 V	60 V

4.5 Ejecting the ions

In order to eject the ions, the final 4 rings will create an electric field gradient accelerating the ions forward from the meeting point to the drift tube the is 16 mm away from the ion guide. As soon as the ions are in the tube, a 2500V pulse will be applied to focus and accelerate the ions. The timing of this pulse is crucial. If the pulse is too early, ions will bounce back from the tube and won't be injected into the MR-ToF MS. If the pulse is too late, the ions will not be focused and accelerated. To determine the right timing, the time-of-flight was measured from the moment the ejection is initiated to the moment the ions reach the center of the tube without any pulse. For Md^{1+} the average time is 4.077μs and for Md^{2+} it is 2.882 μs.

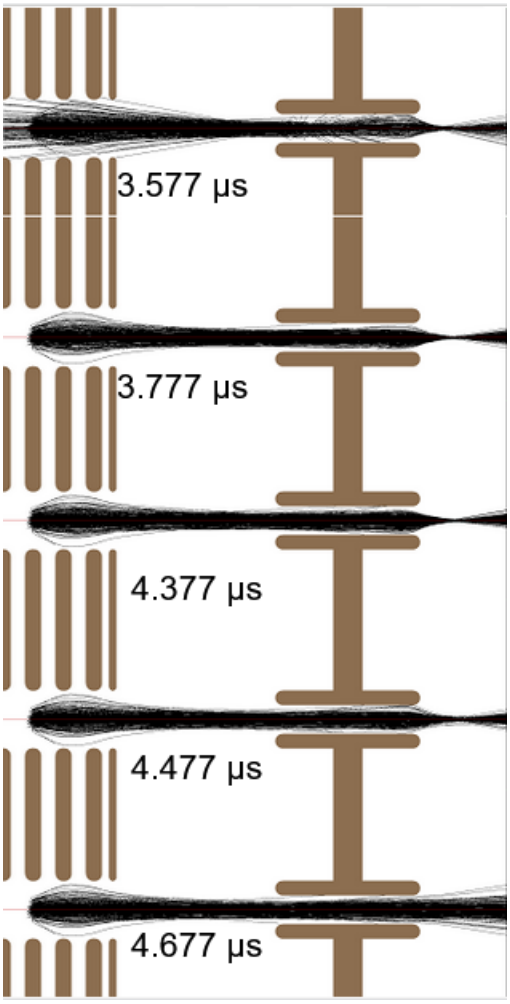

Figure 16: Trajectories of the ion ejection of Md^{1+} ions from the ion guide for various timing of the voltage pulse applied at the drift tube

In practise, the tolerance of the timing was investigated by considering the trajectories of the ions as they pass through the tube. The timings that were tested every 0.1 μs starting from the calculated average. Figure 16 shows the trajectories of 300 Md^{1+} ions as they are ejected at 5 different values for the pulse timing. If the pulse is activated before 3.677μs some ions will bounce back. At 4.477μs some ions are not focused and at 4.677μs none of the ions are focused. In the range 3.777μs to 4.377μs the trajectories are focused and accelerated, therefore the drift tube pulse should be activated within 4.077$\pm$0.3μs after the ejection sequence. Md^{2+} ions are accelerated faster by the ejection sequence, therefore more precision is required to focus and accelerate these. According to the simulations, the drift tube pulse should be activated within 2.882$\pm$0.2μs for Md^{2+}.

4.6 Impact of positioning the ion guide

The transmission rate of the ion guide is dependent on the placement of the ion guide relative to the gas catcher and drift tube. This section is about how shifting the ion guide in both the radial and axial direction affects the yield (see Figure 16).

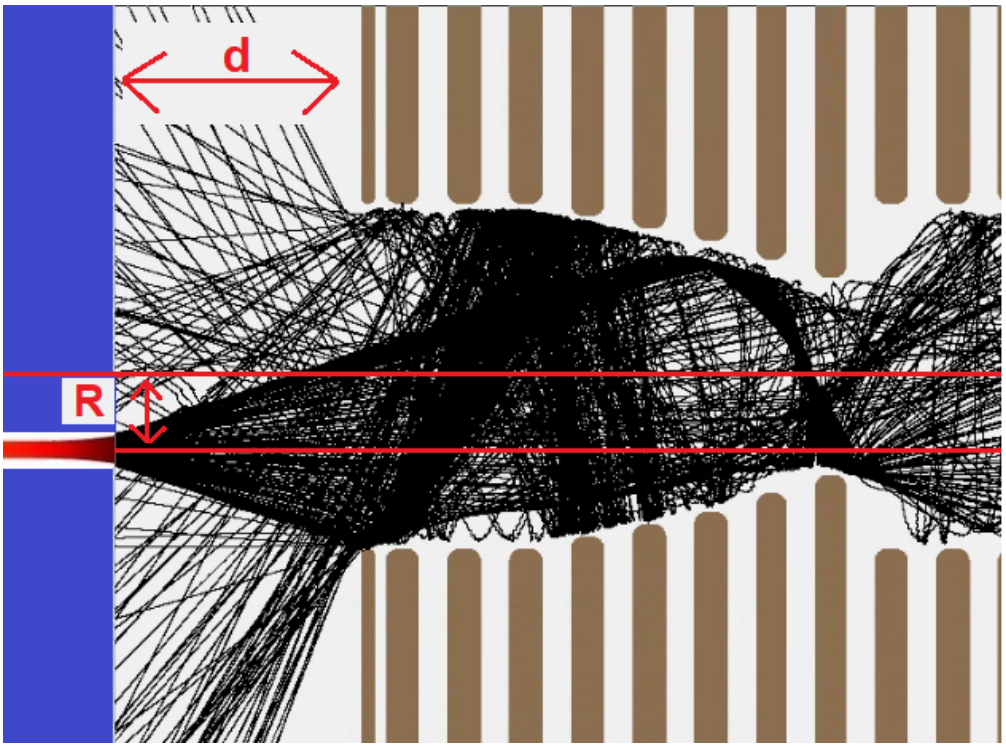

Figure 17: Trajectories of ions being ejected from the gas catcher. for d=10 mm and R=3 mm

4.6.1 Distance from the RF carpet orifice

In systematic studies with Md^{2+} ions, the acceptable distance between the RF carpet and the ion guide was investigated with voltage settings from Table 2. The simulations showed that with the distance in the range of 5 mm to 15 mm, above 95% of the ions ejected from the gas catcher can be captured by the ion guide. The results of this can be seen in Figure 18. These simulations do not take long, therefore 3 simulations were done for each distance. From these simulations, a statistical error was calculated.

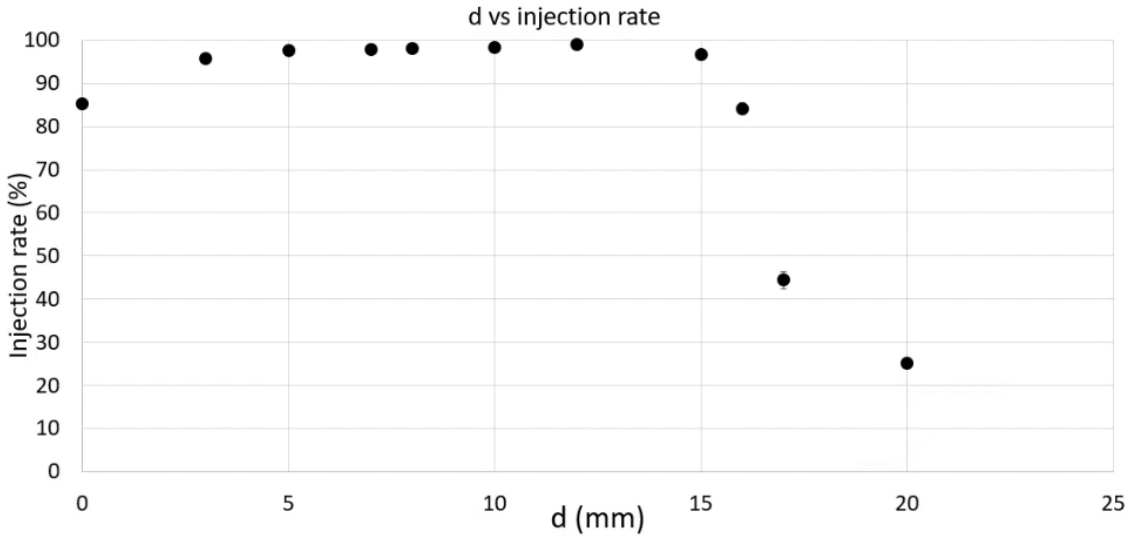

Figure 18: Yield of ions dependent on the distance between RF carpet and ion guide.

4.6.2 Impact of radial misalignment at the injection

For the construction of the ion guide, it is important to know the tolerances of misalignment. To test this tolerance, the ion is radially misaligned with respect to the orifice of the RF carpet. The injection rate was simulated at 5-mm and 10-mm distances between the RF carpet and the ion guide. With Md^{2+} and the voltage settings from Table 2. These simulations do not take long, therefore 3 simulations were done for each distance. From these simulations, a statistical error was calculated.

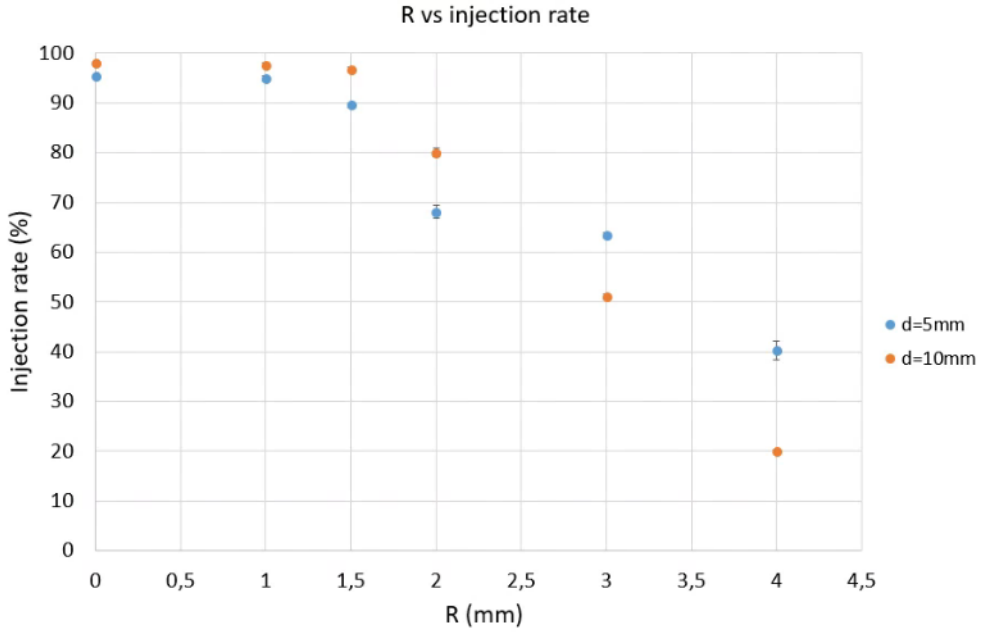

Figure 19: Dependence of the injection yield on the radial misalignment.

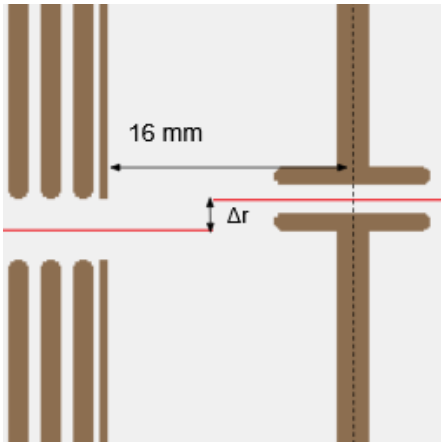

Figure 20: Misaligned drift tube

4.6.3 Impact of a misaligned drift tube

So far the center of the ion guide and the center of the drift tube have been in an ideal line. The real world however may not be ideal, therefore the impact of misalignment has been investigated in simulations. The geometry of the ion guide in SIMION is defined to have cylindrical symmetry, which prevents from offsetting the transverse coordinates of the tube. The tube has an inner radius of 1 mm. The position was recorded for the ions reaching the center of the tube and subsequently checked whether an ion with transverse coordinates (y, z) falls within the boundary of an off-center tube at (-a, -b) in units of millimetres.

$$\sqrt{(y \pm a)^2 + (z \pm b)^2} < 1 \tag{11}$$

If this inequality does not hold for an ion, it means that it will collide with the tube or miss the entrance entirely. Figure 22 shows the percentage of ions that can get through, depending on Δr.

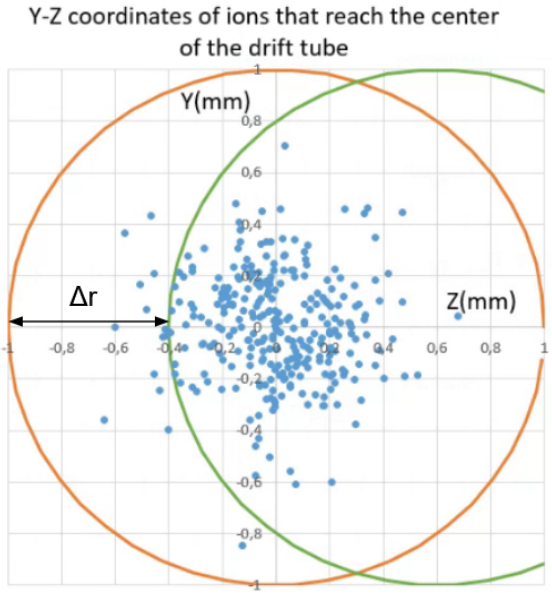

Figure 21: Cross-section of the drift tube at the center. Blue dots indicate where the ions are. The orange circle indicates the boundary of the drift tube. The green circle indicates the boundary of the drift tube shifted by Δr=0.6 mm.

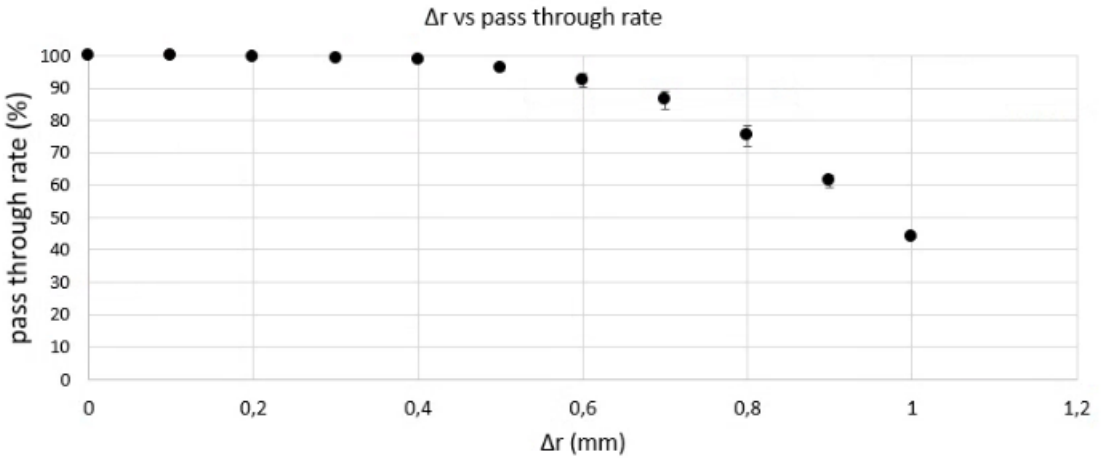

Figure 22: Dependence of the Pass through rate on the radial displacement of drift tube

5 Conclusion

5.1 Electrical settings

From the simulations, it can be concluded that the ion guide is able to transport mendelevium ions at around 90% efficiency using the settings from Table 4. That was simulated using ions with a kinetic energy of 2.6 eV to 2.68 eV. Similar results can be expected if the kinetic energy of the ions is anywhere from 2.4 eV to 3.0 eV. These settings produced the best transmission efficiency in the simulations that were done. Settings with higher efficiency probably exist however due to the long time required to do these simulations, this was not investigated further once 90% transmission efficiency was reached.

Table 4: The recommended settings of the ion guide for each ion

Ion	Confining voltage	Travelling wave voltage	Threshold voltage	RF frequency	drift tube timing
$^{261}Md^{1+}$	105.47 V	2.5 V	2.0V	3.82 MHz	4.077 μs
$^{261}Md^{2+}$	52.735 V	1.25 V	1 V	3.82 MHz	2.882 μs

5.2 Mechanical tolerances

If the placement of the ion guide falls within the ranges from Table 5 at most 10% of ions are lost due to misalignment. Building the ion guide outside these ranges will result in a lower yield. The upper limit of the distance between the RF carpet and the ion guide is 10 mm and not 15 mm because the impact of radial misalignment at that distance was not tested. If the ion guide is built at a different distance, additional testing is needed.

Table 5: Mechanical tolerances of the ion guide

	Range (mm)
Distance from the RF carpet, d	5 to 10
Radial misalignment at the injection, R	<1.5
Radial misalignment at the ejection, Δr	<0.4

In conclusion, simulations were done to study the electrical settings and mechanical tolerances for a novel ring-based ion guide. Electrical settings that transmit 90% of the mendelevium ions were found. The mechanical tolerance of the apparatus was also investigated, which can be used as a guideline for manufacturing the ion guide and placing it inside the NEXT setup.

Acknowledgments

I would like to express my gratitude towards everyone who has helped make this possible. A special thanks goes out to dr. Xiangcheng Chen who helped explained his SIMION code and was always available for questions, dr. Julia Even who supervised this project and Arif Soylu who helped get coffee on many occasions.

References

[1] Y. T. Oganessian and V. K. Utyonkov, "Super-heavy element research," Reports on Progress in Physics v78 n3, 2015.

[2] M.-H. Mun, G. Adamian, N. Antonenko, and Y.-O. Lee, "Possibilities of production of neutron-rich md isotopes in multi-nucleon transfer reactions," The European Physical Journal A 52, 363 (2016). [Online]. Available: https://doi.org/10.1140/epja/i2016-16363-y

[3] J. Kratz, W. Loveland, and K. Moody, "Syntheses of transuranium isotopes with atomic numbers z≤103 in multi-nucleon transfer reactions," *Nuclear Physics A*, vol. 944, pp. 117–157, 2015, special Issue on Superheavy Elements. [Online]. Available: https://www.sciencedirect.com/science/article/pii/S0375947415001335

[4] X. Chen, "The next project: A step to the neutron-rich side," Mainz Actinide Workshop, 26-05-2021.

[5] F. Kondev, M. Wang, W. Huang, S. Naimi, and G. Audi, "The NUBASE2020 evaluation of nuclear physics properties," *Chinese Physics C*, vol. 45, no. 3, p. 030001, mar 2021. [Online]. Available: https://doi.org/10.1088/1674-1137/abddae

[6] J. Dvorak, M. Block, C. Düllmann, S. Heinz, R.-D. Herzberg, and M. Schädel, "Iris—exploring new frontiers in neutron-rich isotopes of the heaviest elements with a new inelastic reaction isotope separator," *Nuclear Instruments and Methods in Physics Research Section A: Accelerators, Spectrometers, Detectors and Associated Equipment*, vol. 652, no. 1, pp. 687–691, 2011. [Online]. Available: https://www.sciencedirect.com/science/article/pii/S0168900210019121

[7] A. Mollaebrahimi, B. Anđelić, J. Even, M. Block, M. Eibach, F. Giacoppo, N. Kalantar-Nayestanaki, O. Kaleja, H. Kremers, M. Laatiaoui, and S. Raeder, "A setup to develop novel chemical isobaric separation (cise)," *Nuclear Instruments and Methods in Physics Research Section B: Beam Interactions with Materials and Atoms*, vol. 463, pp. 508–511, 2020. [Online]. Available: https://www.sciencedirect.com/science/article/pii/S0168583X19301338

[8] R. Wolf, F. Wienholtz, D. Atanasov, D. Beck, K. Blaum, C. Borgmann, F. Herfurth, M. Kowalska, S. Kreim, Y. A. Litvinov, D. Lunney, V. Manea, D. Neidherr, M. Rosenbusch, L. Schweikhard, J. Stanja, and K. Zuber, "Isoltrap's multi-reflection time-of-flight mass separator/spectrometer," *International Journal of Mass Spectrometry*, vol. 349-350, pp. 123–133, 2013, 100 years of Mass Spectrometry. [Online]. Available: https://www.sciencedirect.com/science/article/pii/S1387380613001115

[9] D. Gerlich, *Inhomogeneous RF fields a versatile tool for the study of processes with slow ions.* Universität Freiburg, Freiburg, Germany: John Wiley Sons, Inc, 1992.

[10] W. Meng, G. Audi, F. Kondev, W. Huang, S. Naimi, and X. Xing, "The ame2016 atomic mass evaluation (ii). tables, graphs and references," et al 2017 Chinese Physics C 41 030003.